

The Effect of Rapid Revegetation to Prevent the Severe Erosion at the Post-Eruption Volcano

Takao Yamakoshi, Junichi Kurihara, Tsukuba, Japan, yamak226@pwri.go.jp

Hiroshi Suwa, Uji, Japan, suwa@slope.dpri.kyoto-u.ac.jp

Résumé : The effects of revegetation to prevent the severe erosion at the volcanic slope after the eruption are shown through the hydrologic observation in the field. This study focuses on the Unzen volcano, Japan, erupted recently. In the volcano, severe erosion occurred and was treated by aerial revegetation work to mitigate surface erosion. The authors carried out the field observation of the hydrology and the erosion and found the followings. 1) The erodibility of the slope drastically decreased in the next year of the revegetation 2) The temporal increase in the final infiltration capacity is clearly shown. 3) The temporal change in both the erodibility and the infiltration capacity seems to correspond to the increase in the vegetation in the slope. The coincidence implies that the revegetation work causes the decrease in the water and sediment discharge in the next year of its application.

Introduction

Japan has many active volcanoes, some of which erupt occasionally and, in many cases, result in disturbing hydrologic and erosional condition of watersheds. Many works have reported that it resulted in the significant increase in the erosion and sediment discharge in the down streams(e.g. Collins and Dunne, 1986). The Unzen volcano started its eruptive activities in 1990 and lasted for 5 years with occurrences of many pyroclastic flows. The eastern flank of the volcano was thickly covered with pyroclastic deposits. While and after the eruptions, the deposits were severely eroded and resulted in frequent occurrences of debris flows.

Aerial revegetation works had been conducted in the volcano after the cessation of the eruptions. The vegetation began to grow in the scattered area. In this study, water and sediment runoff monitoring was conducted in the volcano at the slope.

Change in the vegetative cover in the volcano after the eruption

Figure 1 shows satellite images in 1996 right after the revegetation and in 1999. The break line shows the extent of the revegetated area, 489ha. That was executed by helicopters to achieve the wide revegetation immediately. The scattered plants are

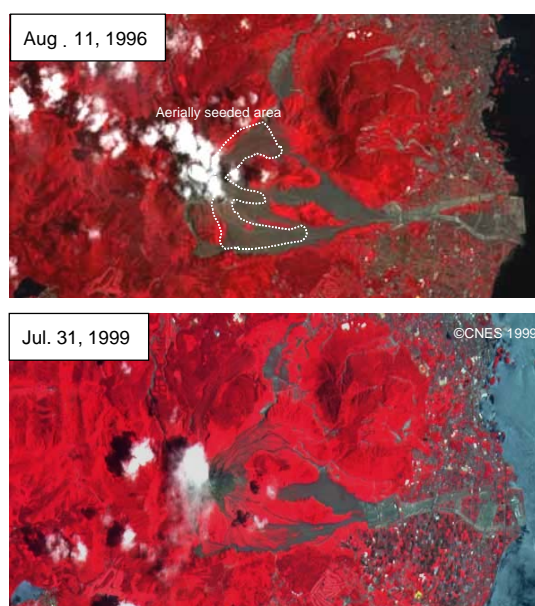


Fig.1 Satellite images of the revegetated areas on the slope of the Unzen volcano in 1996 and 1999 (Aug.1996 : LANDSAT5/TM, Jul.1999 : SPOT2/HRV)

Eragrostis curvula, *Lespedeza bicolor* and others. Photo1 shows the vegetation recovery at the monitoring sites on the pyroclastic flows. Vegetation rapidly began to increase in the next year. The ground surface was almost invisible. After the year 1998, bush came to dominate.

Materials and Methods

The pyroclastic flow deposits has a wide grain size distribution. Sometimes, it includes very large boulder larger than 2m in diameter(see photo.1). The sediment deposited very thickly. The original vegetation was totally buried under the deposit.

The authors conducted the field observation of the hydrology and the eroded sediment. The site was set on the almost center of the vegetated area(Fig.1). The altitude, area and mean slope of the site are 485 m, 280 m² and 20°, respectively. The observation had been conducted between 1996 and 1999.

Yamakoshi and Suwa(2000) has already proposed the simple rainfall-runoff model applicable to the pyroclastic-flow deposits of Mount Unzen. The model describes the runoff process of the Hortonian overland flow, where the effective rainfall is calculated by using a simple tank model with only one virtual drain orifice and one virtual infiltration vent shown in Fig.2. Setting runoff coefficient of the drain orifice to unity, there are just two variable parameters, the height of the drain orifice (H) and the runoff coefficient of the infiltration vent (a).

$$r_{e,i} = \max(h_i - H, 0) \quad (1) \quad h_i = (1 - a)(h_{i-1} - r_{e,i-1}) + r_i \quad (2)$$

where h_i , r_i , $r_{e,i}$ are water level in the tank, rainfall, and effective rainfall at the time step i , respectively. If the tank is fulfilled, the drained rate from the infiltration vent comes to be steady rate, $a \times H$. It corresponds to the hydrological definition of the final infiltration capacity(I_f).

In general, infiltration capacity is not distributed uniformly. For the sake of the simplicity, it is assumed that the slope is divided into two parts, that is, the source area that possesses a certain infiltration capacity and the area of no runoff due to an extremely high infiltration capacity. The proportion of source area is called P_{SA} in this model. The two parts are set

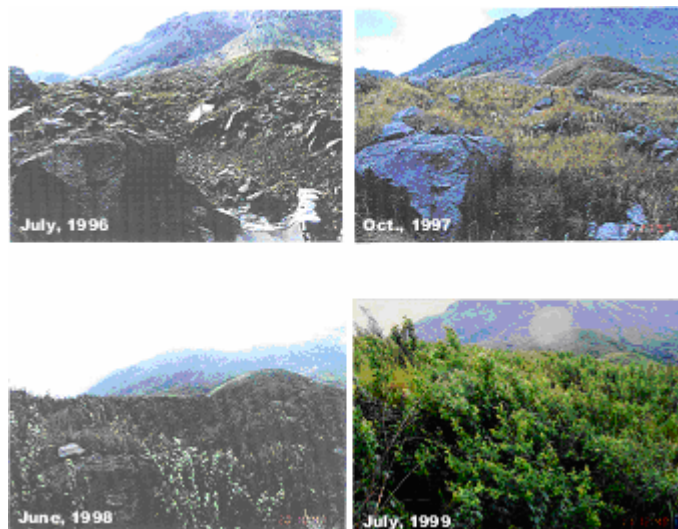


Photo 1 The series of photographs of the vegetation condition at the experimental site

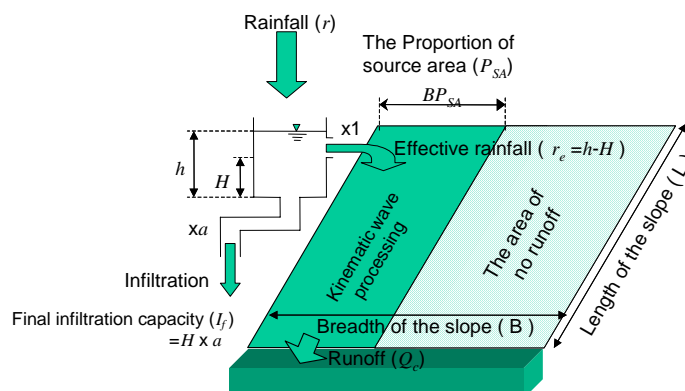


Fig. 2 Schematic illustration of the rainfall-runoff model

The model describes the runoff process of the Hortonian overland flow, where the effective rainfall is calculated by using a simple tank model with only one virtual drain orifice and one virtual infiltration vent shown in Fig.2. Setting runoff coefficient of the drain orifice to unity, there are just two variable parameters, the height of the drain orifice (H) and the runoff coefficient of the infiltration vent (a).

parallel to each other and normal to contours (Fig. 2). The kinematic-wave calculation generates the water discharge at the end of the slope. The optimum set of the demanded parameters, a or I_f , H , and P_{SA} , to mimic the real runoff in this model is searched for all the observed rainfall-runoff events from 1996 to 1999.

Sediment discharge is dependent both on the erosivity and the erodibility. According to Meyer and Wischmeier(1969), the transport capacity is proportional to the 5/3 power of the water discharge. To assess the temporal change in the erodibility of the monitoring site, therefore, the erodibility index (E) is proposed as follows.

$$E = \frac{S}{\sum Q_w^{5/3}} \bigg/ \frac{S_{1996July}}{\sum Q_{w1996July}^{5/3}} \quad (3)$$

The indices for each period are obtained through being normalized by the index in the first month. S is the amount of the monthly sediment deposit and $S_{1996July}$ is that in the first month. Q_w is the observed water runoff rate and $Q_{w1996July}$ is that in the first month.

Results

Figure 3 shows the monthly amount of the rainfall, water runoff and specific sediment discharge. It shows the decrease in the sediment discharge. However, the year 1997 was the unusually rainy year. This fluctuation in the annual rainfall masks the clear temporal change in the water runoff and sediment discharge.

The simulated hydrograph for the case on Sept. 7, 1997 is shown in Fig.4. It is clear that the simple rainfall-runoff model can precisely mimic the real water runoff. The optimum parameters are searched for the 18 rainfall-runoff events from 1996 to 1999. The obtained optimum parameters are shown in Table 2. The temporal change in the final infiltration capacity and the proportion of the source area are shown in Fig. 5. The parameters show almost monotonic temporal change without the effect of the great fluctuation in the annual

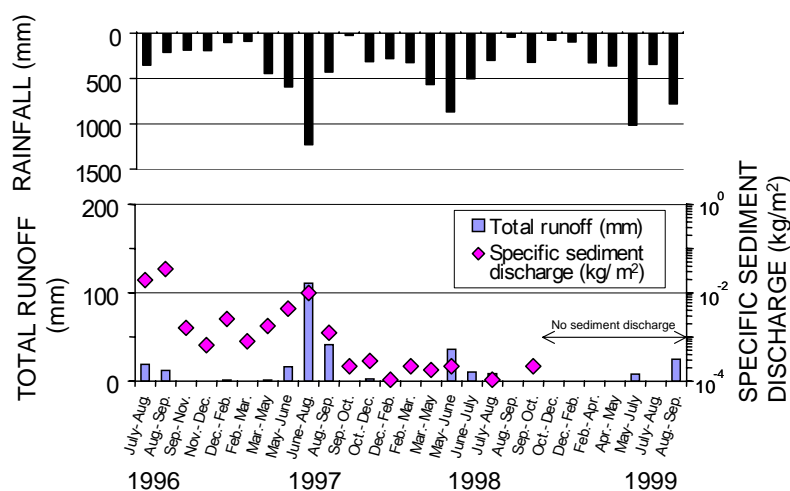


Fig. 3 Monthly rainfall, water runoff, and specific sediment discharge observed at the monitoring site

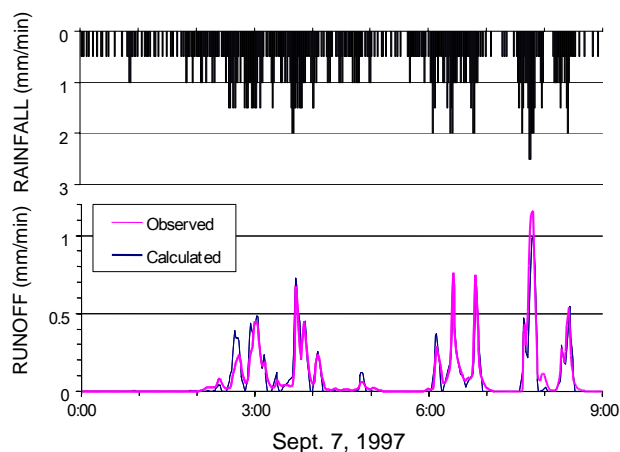


Fig. 4 Observed and calculated hydrographs of the event on Sept. 7, 1997.

Table 2 Optimum parameters

Date	I_f (mm/hr)	P_{SA}	H (mm)
7/19/96	15	0.5	2.5
8/14/96	15	0.35	9.9
8/31/96	9	0.65	16.9
9/ 9/96	12	0.5	10.1
5/13/97	12	0.25	6.9
6/ 8/97	30	0.55	3.7
6/28/97	15	0.5	8.9
8/ 6/97	27	0.95	4.9
9/ 7/97	30	0.55	2.1
11/25/97	27	0.45	9.3
6/ 2/98	30	0.35	11.7
6/13/98	27	0.4	10.5
6/19/98	30	0.4	12.9
6/22/98	39	0.6	0.9
7/25/98	24	0.4	12.1
6/29/99	24	0.15	14.5
7/ 2/99	18	0.15	13.0
9/10/99	24	0.3	13.0

rainfall. Especially the final infiltration capacity significantly increases in the year 1997 in which vegetation started to recover considerably.

The normalized erodibility index is obtained as shown in Fig.6. If the sediment discharge had decreased solely because of the reduce in the water runoff, namely the transport capacity, the indices obtained through the observation period would have shown no temporal change. However, the drastic decrease was found in 1997. It clearly shows that the erodibility of the slope actually decreased over the two orders of its value and the decrease occurred most significantly in 1997, the next year of the revegetation.

Discussion and conclusions

As a result of the application of the proposed rainfall-runoff model and the erodibility index, the temporal change in the hydrologic conditions and the erodibility of the volcanically disturbed and then artificially revegetated slope are clearly shown. It is pointed out that the most significant temporal change in the final infiltration capacity and the erodibility of the slope appeared in 1997, in which the vegetation began to cover the slope significantly. This coincidence implies that the revegetation had an effect to reduce water runoff and the erodibility of the slope. In addition, it is remarkable that the effect appeared instantaneously in the next year of its application.

The previous study showed that the rainfall threshold for the occurrence of debris flows in the river draining the pyroclastic flow deposits rose after the year 1997. The corresponding increase in the infiltration capacity of the revegetated area which occupied the most of the drainage basin of the river seems to imply that the revegetation have a contribution to reduce the debris flow disasters to some extent. However, it is necessary to evaluate the basin-wide effect of the revegetation carefully.

Literature cited

- Collins, B. D. & Dunne, T. (1986) : Erosion of tephra from the 1980 eruption of Mount St. Helens, Geol. Soc. Am. Bul., 97, pp.896-905.
 Yamakoshi, T. and Suwa, H. (2000) : Post-eruption characteristics of surface runoff and sediment discharge on the slopes of pyroclastic-flow deposits, Mount Unzen, Japan, Trans. Japanese Geomorph. Union, 21-4, pp.469-497.
 Meyer, L.D. and Wischmeier, W.H. (1969) : Mathematical simulation of the process of soil

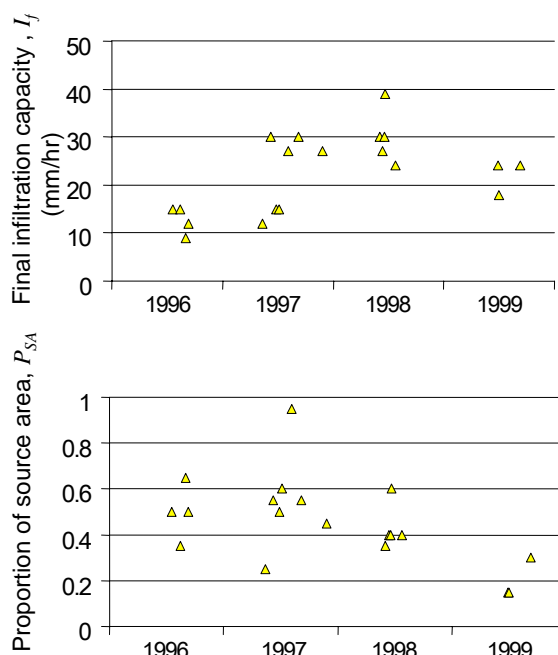


Fig.5 Temporal change in the acquired optimum hydrologic parameters at the observation site.

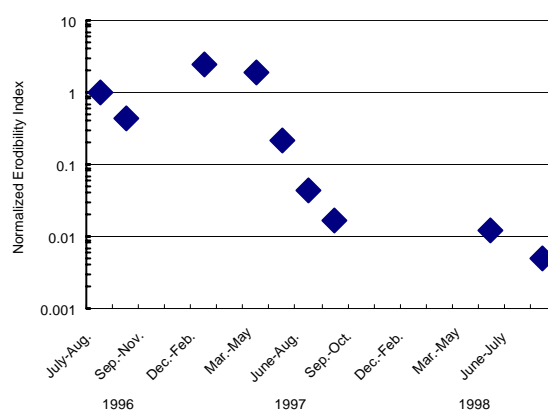


Fig.6 Temporal change in the normalized erodibility index of the observation site

erosion by water. Trans. ASAE, 12, 754-758.